International Journal of Biological Macromolecules 234 (2023) 123693

Contents lists available at ScienceDirect

International Journal of Biological Macromolecules

journal homepage: www.elsevier.com/locate/ijbiomac

Fabrication and characterization of PVA@PLA electrospinning nanofibers embedded with *Bletilla striata polysaccharide* and *Rosmarinic acid* to promote wound healing

Guofeng Zhong [a,1], Mengyu Qiu [a,1], Junbo Zhang [a], Fuchen Jiang [a], Xuan Yue [a], Chi Huang [a], Shiyi Zhao [a], Rui Zeng [b], Chen Zhang [a,*], Yan Qu [a,*]

[a] State Key Laboratory of Southwestern Chinese Medicine Resources, School of Pharmacy, Chengdu University of Traditional Chinese Medicine, Chengdu 611137, China
[b] College of Pharmacy, Southwest Minzu University, Chengdu 610041, China

ARTICLE INFO

Keywords:
Bletilla striata polysaccharide
Rosmarinic acid
Coaxial electrospinning
Wound dressing

ABSTRACT

In this study, a novel nanofiber material with *Polylactic acid* (PLA), natural plant polysaccharides-*Bletilla striata polysaccharide* (BSP) and *Rosmarinic acid* (RA) as the raw materials to facilitate wound healing was well prepared through coaxial electrospinning. The morphology of RA-BSP-PVA@PLA nanofibers was characterized through scanning electron microscopy (SEM), and the successful formation of core-shell structure was verified under confocal laser microscopy (CLSM) and Fourier transform infrared spectroscopy (FTIR). RA-BSP-PVA@PLA exhibited suitable air permeability for wound healing, as indicated by the result of the water vapor permeability (WVTR) study. The results of tension test results indicated the RA-BSP-PVA@PLA nanofiber exhibited excellent flexibility and better accommodates wounds. Moreover, the biocompatibility of RA-BSP-PVA@PLA was examined through MTT assay. Lastly, RA-BSP-PVA@PLA nanofibers can induce wound tissue growth, as verified by the rat dorsal skin wound models and tissue sections. Furthermore, RA-BSP-PVA@PLA can facilitate the proliferation and transformation of early wound macrophages, and down-regulate MPO^{+} expression of on the wound, thus facilitating wound healing, as confirmed by the result of immunohistochemical. Thus, RA-BSP-PVA@PLA nanofibers show great potential as wound dressings in wound healing.

1. Introduction

The skin is the greatest organ on the surface of the human body that contacts the outside world. It is capable of the functions of resisting microorganisms, regulating body temperature, and resisting external environmental stimuli. However, it has always been exposed to dangerous environments, (e.g., burns, frostbite and acute damage by sharp instruments); it reduces the wound healing rate and causes the loss of skin function under the effect of bacterial infection [1,2]. Wound healing refers to a continuous process. At the inflammatory stage, it primarily removes damaged or dead wound tissue, whereas the neutrophils will release numerous of reactive oxygen species (ROS), thus damaging the epithelial cells; as a result, the secretion of inflammatory cytokines can be facilitated [3]. Lastly, it creates a vicious cycle of wound inflammation. It can be a huge mental burden on the patients. Accordingly, therapeutic approaches are required to facilitate wound healing while reducing wound inflammatory responses.

Electrospinning has become extensively used over the past few years in a variety of industries, (e.g., food packaging, artificial intelligence, medicine delivery, tissue engineering, and wound dressings) [4–10]. Wound dressings prepared from electrospun nanofibers exhibit a smooth surface and similarity to the architecture of the natural extracellular matrix (ECM) in comparison with conventional dressings, such that they can facilitate cell adhesion, while enveloping and protecting a variety of bioactive substances [11]. The most common electrospinning methods of electrospinning are classified into uniaxial and multi-axis. Uniaxial electrospinning methods have a single structure, which may cause rapid dissociation of effective materials and drugs, reducing their biological activity. However, multi-axis electrospinning technology is to spin different materials through various channels to form a core-shell

* Corresponding authors at: State Key Laboratory of Southwestern Chinese Medicine Resources, Chengdu University of Traditional Chinese Medicine, Chengdu 610072, China.
E-mail addresses: chenzhang_1990@126.com (C. Zhang), quyan028@126.com (Y. Qu).
[1] These authors have contributed equally to this work.

https://doi.org/10.1016/j.ijbiomac.2023.123693
Received 2 December 2022; Received in revised form 3 February 2023; Accepted 11 February 2023
Available online 17 February 2023

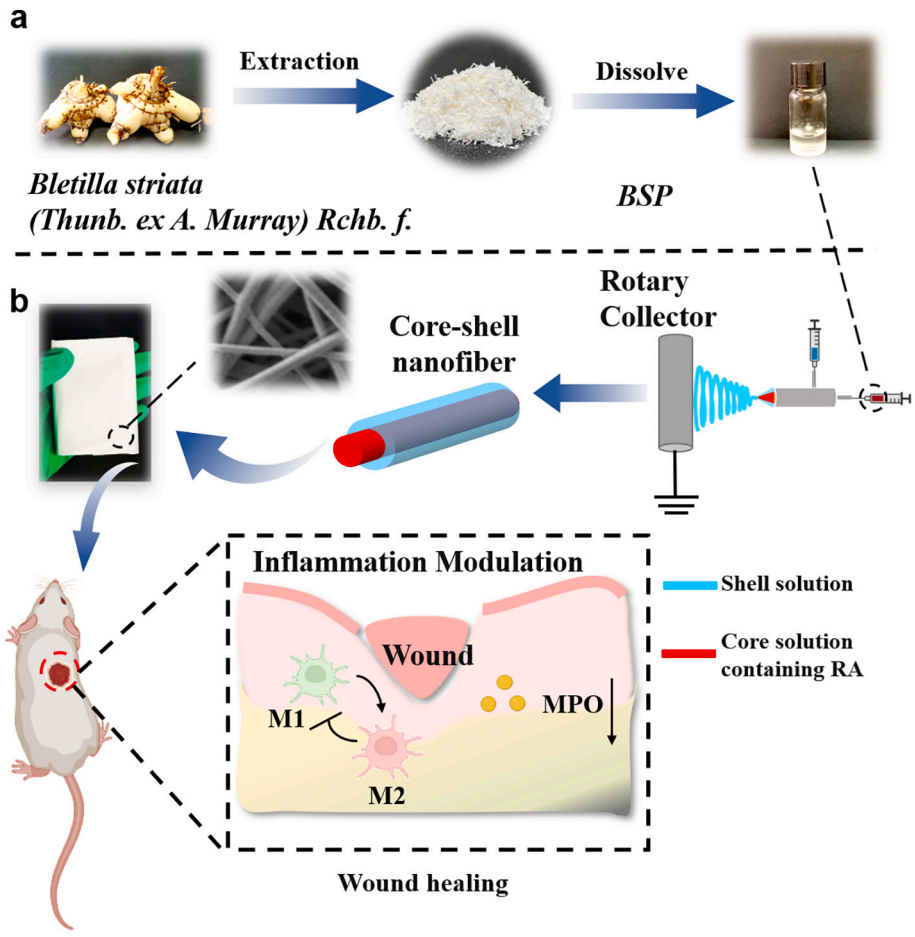

Scheme. 1. Schematic diagram of RA-BSP-PVA@PLA coaxial nanofiber design strategy. (A) Preparation and application of RA-BSP-PVA@PLA nanofibers, extraction and preparation of BSP. (B) Schematic diagram of preparation of coaxial nanofibers and their promotion of wound healing.

structure, thus decreasing the dissolution rate of effective materials and medicines and maintaining their biological activities [12,13].

Existing research has suggested that natural polymers and synthetic polymers can be employed for electrospinning [14,15]. The natural polymer is capable of inducing cell adhesion and growth [16], thus achieving the biological activity of the natural polymer itself. Natural plant polysaccharides have been extensively employed in the biomedical field over the past few years [17–20]. BSP refers to a type of natural plant polysaccharide. It is extracted from *Bletilla striata (Thunb.)* of plant, comprising α-mannose, β-glucose, and β-mannose. Besides, it has aroused wide interest for its functions of promoting skin healing, anti-inflammation, and anti-fibrosis, as well as its excellent biocompatibility, biodegradation, and low cost. It can also apply to hydrogel, sponge, microneedle and other medical materials [21–27]. Based on the above-described findings, BSP was selected as one of the effective materials in the nuclear layer in this study, whereas, its spinnability is poor, PVA has been already widely applied in biomedicine as a safe, biodegradable polymer [28], such that PVA was added as a support material to enhance the spinnability of the nuclear layer [29,30]. Synthetic polymers can apply to electrospinning nanofibers to enhance the mechanical properties of nanofibers, and they can adapt to wounds of different sizes [31], (e.g., PLA, Polyethylene glycol (PEG), Poly (lactic-co-glycolic acid) (PLGA), and Polycaprolactone (PCL) [32–34]). PLA has been confirmed as one of the most used bioplastics worldwide. Furthermore, it is a safe, non-toxic material exhibiting excellent biocompatibility, degradability, and suitable mechanical properties, and it has been applied in a wide range of fields of biomedicine [35,36]. Thus, PLA was selected as the on-shell part of coaxial nanofiber.

RA refers to a natural polyphenolic carboxylic acid, a major component of a variety of medicinal ingredients and proprietary Chinese medicines, with different potential biological properties. (e.g., antioxidant and anti-inflammatory properties [37–39]). However, RA is susceptible to light and oxygen and readily breaks down, such that reactive oxygen species scavenged at the inflammatory phase exhibit insufficient capacity. Thus, coaxial ele2ctrospinning techniques can be used to protect RA biological activity, reduce wound inflammation, and promote wound healing.

In this study, we created a core-shell nanofiber with BSP-PVA@PLA as a scaffold to load RA into the nuclear layer and exert anti-inflammatory and promote wound healing effects (Scheme. 1). The characteristics of this study are as follows: (1) In order to ensure the bioactivity of RA and BSP, RA and BSP were loaded into PVA@PLA coaxial nanofibers to reduce the degradation rate of RA and BSP; (2) BSP and RA in the nuclear layer improve the flexibility and mechanical strength of wound dressing; (3) RA-BSP-PVA@PLA has great protective effect and gas permeability, and because PLA has excellent hydrophobic performance, it keep the wound moist environment, such that it can facilitate wound healing [40,41]; (4) BSP and RA are capable of inducing the polarization of M1-type macrophages to M2-type macrophages in wounds [42–44], which speeds up wound healing; (5) RA and BSP in the nuclear layer can reduce wound inflammation, thus promoting wound healing [45–47].

2. Experimental section

2.1. Materials

Sichuan provided Dried *Bletilla striata* (B.striata) was purchased from Sichuan Chinese Medicine Yinpian Co., Ltd. (Sichuan, China). Rosmarinic acid was purchased from Chengdu Durst Biotechnology Co., LTD., Polylactic acid (PLA, molecular weight = 80.000 W) and FITC were obtained from Aladdin. Polyvinyl alcohol (PVA, Chengdu Cologne Chemical Reagent Company), Chengdu Cologne Chemical Reagent Company provided the chloroform (99.0 %) and *N*, *N*-dimethylformamide (DMF, >99.9 %). Thiazolium blue (MTT) (Biofroxx, Germany), dimethyl sulfoxide (DMSO) (MP Biomedicals, France), Hoechst 33258 staining solution (Shanghai Baissey Biotechnology Co., LTD., China). All animals were purchased from SPF (Beijing, China) Biotechnology Co., Ltd., the ambient temperature is 23 ± 2 °C; the relative humidity is 55 ± 5 %; 12 h light/dark cycle. Throughout the entire trial, the animals had unrestricted access to tap water and standard rat chew, and the beds were changed out three times per week. Following the recommendations for the handling and use of laboratory animals issued by the National Institutes of Health in the United States, all animal experiments were given the go-ahead by the Experimental Animal Protection Society of Chengdu University of Traditional Chinese Medicine.

2.2. Preparation of coaxial nanofiber

2.2.1. Preparation of BSP

BSP was created in the lab in accordance with the instructions of the manufacturer [48]. The tuber of *Bletilla striata* was powdered. Subsequently, ethanol (95 %) and petroleum ether (60–90 °C) degree were used at 70 °C for 2 times, 2 h each time, according to the solid-liquid ratio of 1:5 (m/v). The medicinal powder was re-weighed and added into deionized water according to the solid-liquid ratio of 1:40, the powder was stirred at 70 °C for 2 h, then filtered and concentrated extract. The protein was removed using a 1/3 Sevage reagent, and the aqueous phase was subsequently collected. After cooling, 95 % ethanol was added, and the polysaccharide was precipitated by stirring the alcohol at a low speed. The polysaccharide was refrigerated at 4 °C for 12 h, filtered, and then washed. BSP was purified with the DEAE Cellulose 52 columns (6.0 cm × 55.0 cm). The monosaccharide content and the purity of the BSP were determined using the reverse-phase HPLC and HPGPC.

2.2.2. Coaxial electrospinning solution preparation

For the nuclear layer solution, 10 % (*w/v*) PVA was dissolved in deionized water. After the solution was fully dissolved, BSP (7.5 %, w/v) and RA (2 mg/mL) were added and dissolved by magnetic stirring until the nuclear layer solution PVA-BSP-RA was obtained. Furthermore, the PLA shell solution was prepared by dissolving PLA 10 % (*w/v*) particles in chloroform/DMF (8:2, *v*/v) and stirring on a magnetic stirrer for 24 h.

2.2.3. Coaxial electrospinning technology

A coaxial spinning needle with a 20-gauge needle core and a 10 mL syringe filled with polymer was connected with a 17-gauge needle housing. The flow rates were 0.06 mL/h and 0.5 mL/h for the core and shell at 16 kV voltage, a sheet of aluminum foil was placed on a drum collector with a diameter of 15 cm at a speed of 150 rpm for collection. Likewise, the PVA@PLA and BSP-PVA@PLA coaxial nanofibers were prepared.

2.3. Confocal laser scanning microscopy (CLSM)

FITC 2 mg and rhodamine powder 1 mg were accurately weighed and then placed in PLA and RA-BSP-PVA solutions, respectively, and spun according to the same method as above. After completion, the collected coaxial nanofibers were placed under a confocal laser scanning microscope (DM6B, Leica, Germany) to characterize the fiber structure.

2.4. Scanning electron microscope (SEM)

The coaxial nanofibers were examined using SEM (Axio Imagerm2 EVO10, Germany). The coaxial nanofibers samples were gilded with a sputter gilding machine for 40 s prior to observation. The diameters of 100 distinct nanofibers were randomly selected and determined using Image J software (National Institutes of Health).

2.5. Transmission electron microscope (TEM)

The samples were tested using TEM (TEMH7800, Hitachi, Japan) at an operating voltage of 120 kV to demonstrate the core-shell structure of the samples. Moreover, a layer of carbon-coated copper mesh was fixed to the collector for the preparation of the coaxial nanofiber sample prior to observation.

2.6. Fourier transform infrared spectroscopy (FTIR)

FTIR spectroscopy was performed using a Spectrum One Fourier transform infrared spectrometer (PerkinElmer, USA) to determine the molecular characteristics of several materials (PLA, PVA, BSP, RA, and three coaxial nanofibers). The above-mentioned samples were ground using three coaxial nanofiber samples. Subsequently, the powder was compacted into disks of transparent potassium bromide for scanning in a range of 4000–500 cm^{-1}.

2.7. Water contact angle measurement

The water contact angle (WCAS) was tested using a video optical contact goniometer (OCA25, dataphysics, Germany) to determine the hydrophobicity after the coaxial nanofibers were divided into 5 cm × 5 cm.

2.8. Water vapor transmittance

The WVTR of coaxial nanofibers was examined through gravimetry [49]. The glass bottle was filled with 5 mL of deionized water, and the nanofibers were attached to the mouth of the glass bottle with a diameter of 1.2 cm. The control group was open glass bottles. The glass bottles were placed in a desiccator at 25 °C for 24 h. Measure the weight of the glass bottle at intervals. Three times the experiment was run. The following formulae are used to determine the WVTR:

$$\mathrm{WVTR}\ (\%) = \mathrm{W0} - \mathrm{Wt}/\mathrm{A} \times 100\% \quad (1)$$

Here W0 and Wt are the initial and final weights of the glass bottle, respectively. A is the area of the opening of the glass bottle.

2.9. Tensile strength

The samples mechanical strength was examined with a texture analyzer (Rapid TA+, Shanghai Tengba Instrument Technology Co., LTD.). The prepared coaxial nanofiber sample (50 mm long x 10 mm wide) was fixed with two clamps and measured at 0.2 mm/s. Furthermore, the stress-strain curves were recorded for RA-BSP@PLA, BSP@PLA, as well as PVA@PLA nanofibers.

2.10. Biocompatibility test

2.10.1. Apoptosis assay

A total of three distinct coaxial nanofibers were co-cultured with L929 cells for 24 and 48 h using the 24-well plates. After being co-incubated, the samples were fixed with 4 % paraformaldehyde at ambient temperature for 15 min, washed with PBS buffer 3 times, 3 min each time. The cells were stained for 30 min with Hoechst 33258

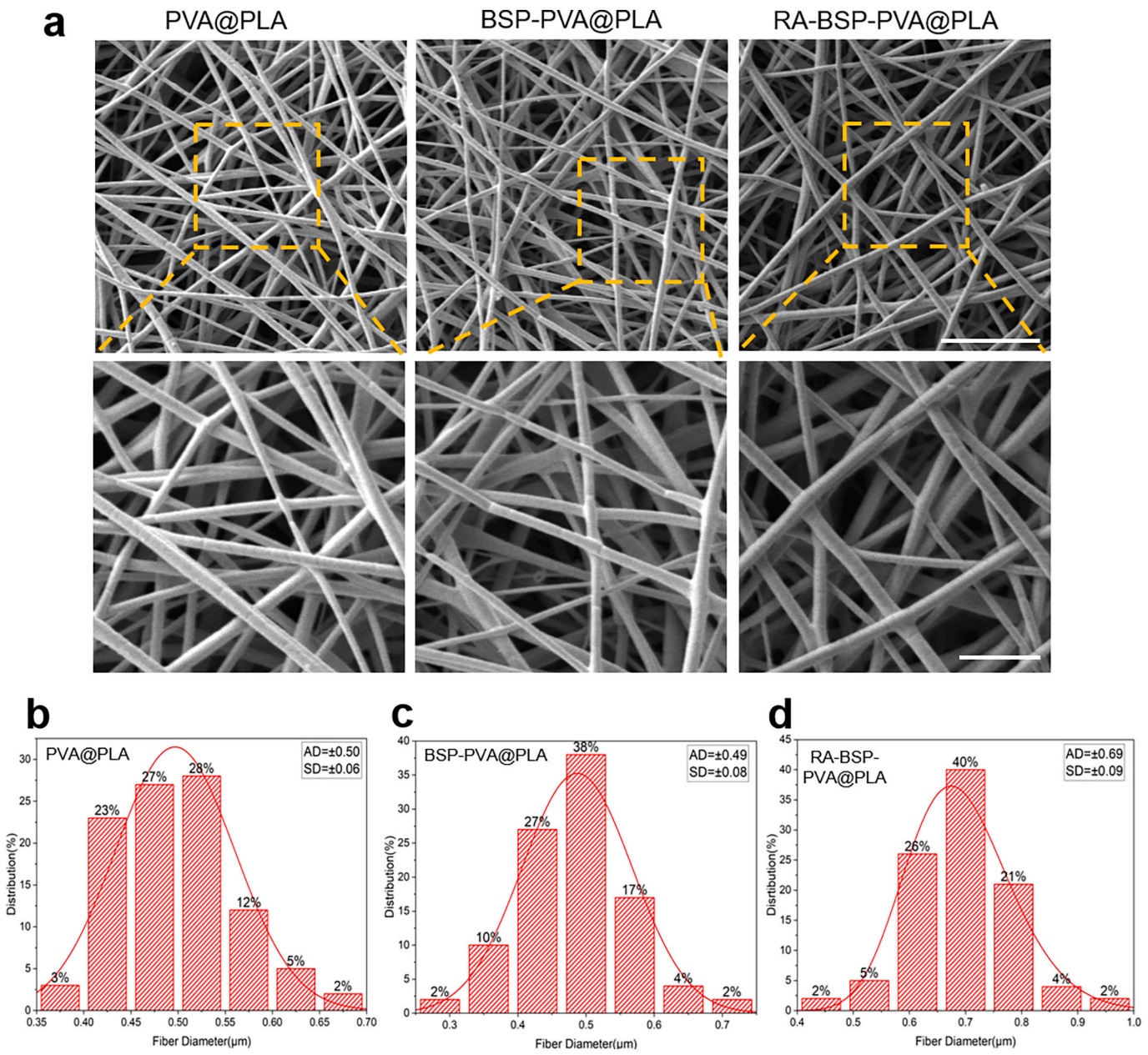

Fig. 1. Coaxial nanofibers appearance and distribution of diameters. (a) SEM images at 1000× and 2000× magnification. Scale bar: 10 μm and 4 μm. (b-d) According to statistics derived from SEM images, the nanofibers' diameter distributions and average diameter ($n = 100$).

staining solution. The cells were stained, and the apoptosis was observed under a fluorescent microscope (Leica, Wetzlar, Germany) (The nuclei of normal cells were light blue, whereas the nuclei of apoptotic cells showed bright blue fluorescence).

2.10.2. MTT

3000 cells were blown into single-cell suspensions using MDEM media supplemented with 10 % fetal bovine serum and 1 % dual antibody to seed L929 cells into 96-well plates. Different coaxial line nanofibers were inserted and then treated for 24, 48, or 72 h, respectively, after being incubated for the first 24 h. After the treatment, 100 μL of fresh media and 10 μL of MTT solution were added, and the mixture was incubated for 2 h with the old medium removed. After the culture was completed, the supernatant was carefully taken out, 150 μL of DMSO was added to the respective well, and the crystals were thoroughly dissolved by shaking for 15 min., The absorbance of the respective well was measured at 490 nm on a microplate reader (Thermo Fisher Scientific, Ulm, Germany), and cell viability was determined.

2.10.3. Cell morphology experiment

A wide variety of coaxial nanofibers were added after 24 h of CO2 incubator incubation and cell seeding in 24-well plates. Subsequently the cells were incubated for another 24 or 48 h. After treatment, the cells' morphological alterations were examined under a microscope (Leica, Wetzlar, Germany).

2.11. Wound healing and histopathological analysis

2.11.1. Wound healing

The effect of coaxial nanofibers on the wound-healing process was examined through in-vivo experimental research. Nine male SD rats weighing 200–300 g were selected as the subjects in the experimental research. Pentobarbital was injected intraperitoneally for anesthesia after the rats were randomly assigned to the control and treatment

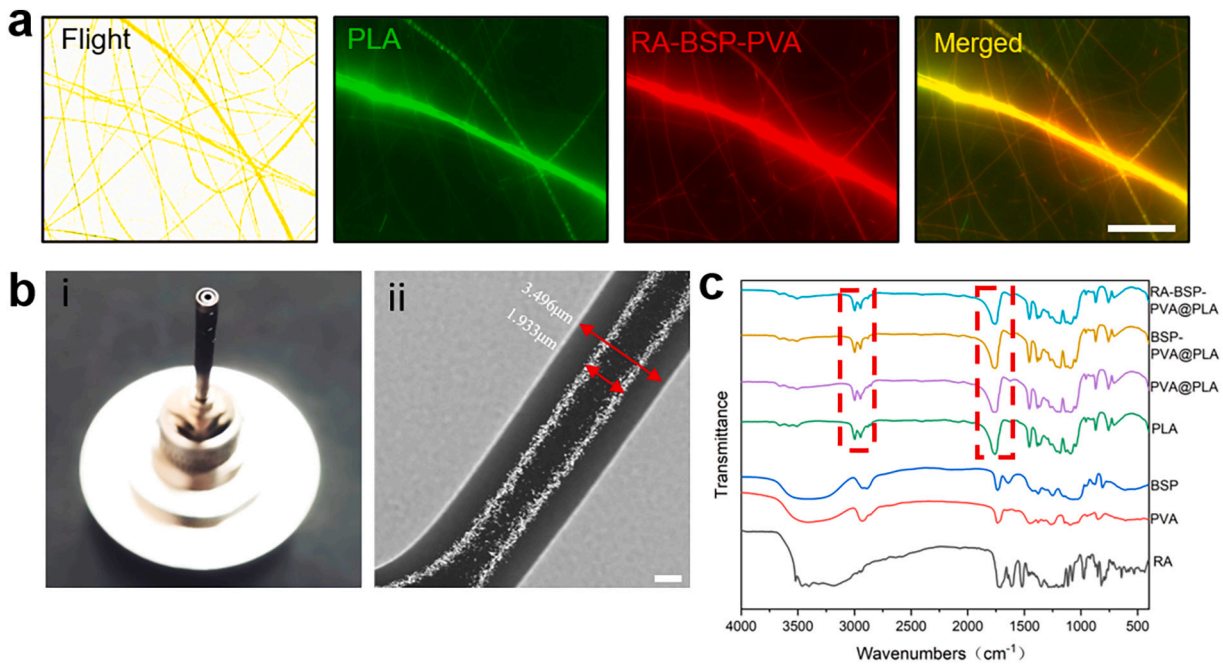

Fig. 2. Coaxial nanofibers structural features. (a) Coaxial nanofibers under the fluorescence microscope. The shell is composed of PLA and stained with FITC (green). The inner layer consists of RA-BSP-PVA and is stained with Rhodamine (red). Scale bar: 50 μm. (b) (i) Schematic diagram of coaxial needle (ii) TEM image of coaxial nanofibers. Scale bar: 1 μm. (c) FTIR spectra of coaxial nanofibers and FTIR spectra of raw materials (RA, BSP, PVA, PLA).

groups. They had their back hair shaved with a razor, leaving a 0.8 cm-diameter circular wound in their flesh. The wounds in the control group were covered with the gauze, while the wounds in the treatment group were healed using coaxial nanofibers. Lastly, the rats were raised individually to track the healing of the wounds, and the wounds were captured at 0, 5, 10, and 15 days. After the wound's size was measured with ImageJ software, the wound closure % was determined as follows:

$$\text{Wound closure}\ (\%) = (\text{Wound area at day } 0 - \text{wound area at day N})/\text{Wound area at day } 0 \times 100\% \quad (2)$$

2.11.2. Histopathological analysis

On days 5, 10, and 15, the rats in each group were put to death, and the wound tissue was removed. For 48 h, the samples were fixed in 10 % paraformaldehyde. The specimens were fixed, viewed under a microscope, embedded in paraffin, and the photographs were gathered and processed. Sections measuring 5 μm each were cut using the microtome. Slices of tissue were stained with hematoxylin and eosin (H&E) and Masson's trichrome (Masson). Rat wounds' histological alterations were then examined under a microscope and captured on camera.

2.12. Immunohistochemical analysis

In wound healing, preventing inflammation is crucial, including inflammatory cytokines secretion and inappropriate macrophage differentiation. It has two kinds of M1, and M2 macrophages phenotype, M1 macrophages in wounds will continue to release proinflammatory factors, and M2 macrophages can accelerate fibroblast proliferation, and anti-inflammation, and promote wound healing. Neutrophils (MPO^+) are the direct expression of inflammatory factors. If MPO^+ increases, it indicates that wound inflammation is continuously developing and increasing, slowing down the process of wound healing [50]. Since both RA and BSP can induce M1 macrophages to transform into M2 macrophages and have anti-inflammatory effects [42–47], the expression of macrophages and the expression level of inflammatory factor MPO^+ were measured after staining of macrophages with FITC and CY3, to evaluate the synergistic effect of RA and BSP in promoting macrophage conversion and anti-inflammatory function.

2.13. Statistical analysis

Origin 2021 was used in a one-way ANOVA with Tukey's post hoc test to evaluate whether there were any significant differences. The statistically significant difference was defined as $P < 0.05$.

3. Results and discussion

3.1. Preparation of BSP

In this experiment, BSP that was isolated from the same batch as that used in our lab was used [25]. According to the experimental findings, BSP comprises mannose and glucose at a ratio of 2.95:1, with (1 → 4)-linked-D-mannose serving as the primary link in the main chain. Purified BSP has Mw and Mn of 3.99×10^5 g/mol and 7.09×10^4 g/mol, respectively. BSP contains 90.18 % carbs in total.

3.2. Morphological characteristics of coaxial electrospinning film

Coaxial electrospinning has certain requirements on the flow rate, concentration, and core-shell ratio of the solution, and the flow rate of the nucleus must be lower than that of the shell [13]. For this reason, the core-to-shell velocity ratio is set to 1: 8.3 in this study. As depicted in

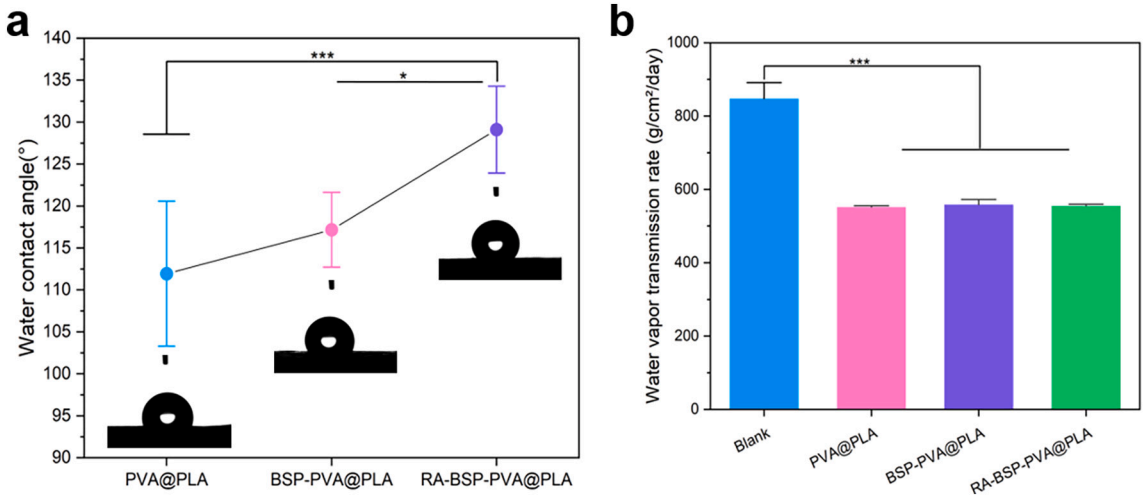

Fig. 3. Water contact Angle and water vapor transmittance. (a) Water contact angles of three different coaxial nanofibers ($n = 3$). (b) Water vapor transmission rate of coaxial nanofibers (n = 3). Data represent mean ± SD; $^{*}P < 0.05$, $^{***}P < 0.001$.

Fig. 1a, the fiber surface was smooth and free of holes, beads, cracks, and other defects, and the fibers were mixed, suggesting that the composition of the core and shell significantly affects the shape of the fiber. The diameter of the PVA@PLA coaxial nanofibers in this study was 0.50 ± 0.06 μm (Fig. 1b), and the diameter distribution range expanded with the inclusion of BSP and RA. The diameter of the BSP-PVA@PLA nanofiber with BSP as its core material was 0.49 ± 0.08 μm (Fig. 1c). When BSP and RA served as the core materials, RA-BSP-PVA@PLA nanofiber exhibited a diameter of 0.69 ± 0.09 μm (Fig. 1d) with a fairly uniform diameter distribution.

Based on the reported approach, rhodamine and FITC fluorescein were added to the core and shell, respectively, to view the core-shell structure in more detail [51], A fluorescent microscope image (Fig. 2a) indicates the distribution of the core-shell structure. The successful realization of the core-shell structure was confirmed through fluorescence measurements.

Fig. 2b(i) illustrates the structure of the coaxial needle device, The analysis of the result of TEM (Fig. 2b(ii)) indicated the structure and morphology of coaxial nanofibers, with the middle layer being black and the outer surface gray.

3.3. FITR analysis

FTIR spectra of polymer and drug samples were analyzed to evaluate

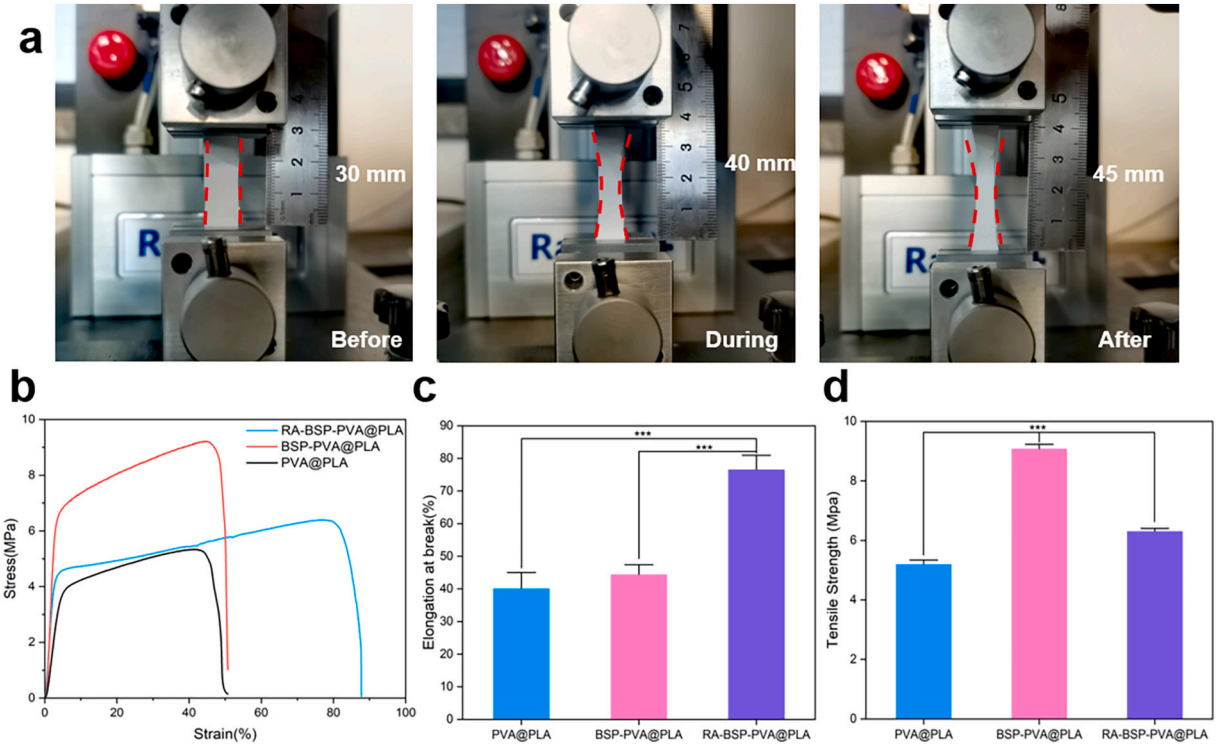

Fig. 4. Mechanical properties of coaxial nanofibers. (a) The optical photos of the stress-strain behavior of RA-BSP-PVA@PLA. (b) Stress-strain curves of coaxial nanofibers ($n = 3$). (c) Extension at peak of three different coaxial nanofibers (n = 3). (d) Tensile strength of three different coaxial nanofibers (n = 3). Data represent mean ± SD; $^{*}P < 0.05$, $^{***}P < 0.001$.

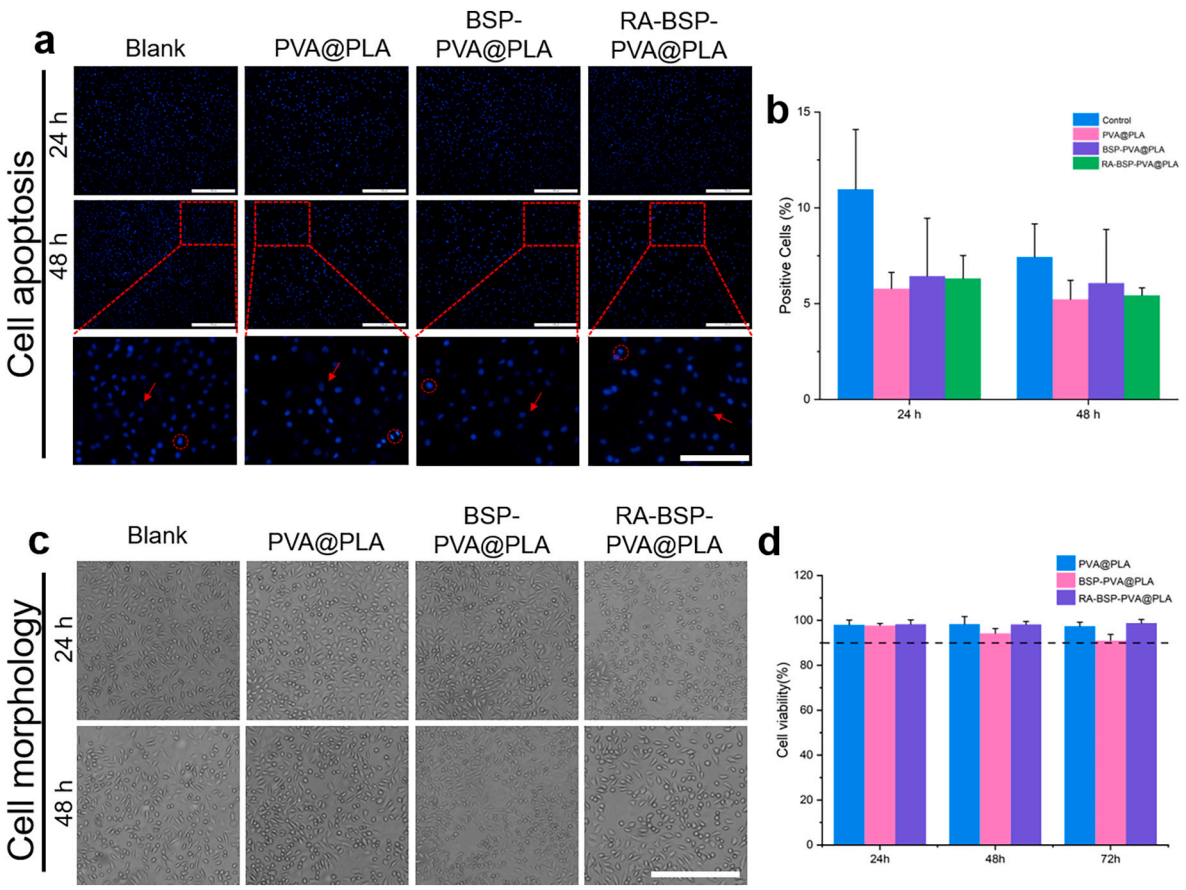

Fig. 5. The cytotoxicity of coaxial nanofibers. (a) Fluorescence of L929 cells after Hoechst 33258 (blue) (Red arrows: living cells, red circles are apoptotic cells) staining ($n = 3$). Scale bar: 100 and 50 μm. (b) Cell apoptosis rate. (c) L929 cell morphology (n = 3). Scale bar: 100 μm (d) The cytotoxicity of coaxial nanofibers to L929. Data represent mean ± SD.

bond formation. Fig. 3c illustrates the FTIR spectra of RA, BSP, PVA, PLA, as well as coaxial nanofibers. The main characteristic peaks of RA were identified at 3399 cm^{-1}(O—H) and 1656 cm^{-1}(C═O stretching vibration) [37]. BSP displayed a characteristic peak at 1633 cm^{-1}(C═O stretching vibration) and 2800-3600 cm^{-1}(O—H stretching vibration), whereas PVA indicated a characteristic peak at 3409 cm^{-1}(O—H stretching vibration). No bands (e.g., PVA, BSP, and RA) were identified in the drug samples. The PLA in the 1500–2000 cm^{-1} and 3000 cm^{-1} correlation regions were highlighted in the three coaxial nanofibers. The characteristic peaks of PVA, BSP, and RA were not identified, suggesting that PVA, BSP, and RA were completely encapsulated in the core layer [52]. On that basis, the formation of the coaxial structure was verified in accordance with the result of confocal microscopy and TEM images. Furthermore, the degradation performance of PLA material was tested (Support information, Fig. S1).

3.4. Water contact angle experiment

The wettability of three kinds of coaxial spinning films was tested by contact angle experiment. Due to the hydrophobicity of the PLA material [53], the solution of BSP and RA in the core can be prevented. The contact angles of PVA@PLA, BSP-PVA@PLA, and RA-BSP-PVA@PLA are 111.93 ± 3.48°, 117.17 ± 1.80° and 129.10 ± 2.08° (Fig. 3a). This may be because the PLA gathered on the surface gradually increased with the increase of the components in the shell, and the hydrophobicity was strong, close to the superhydrophobic surface (150°) [54]. At the same time, droplet formation is seen in all three types of coaxial nanofibers.

3.5. WVTR

Only wound dressings with WVTR between 76 and 9360 g/m^2/ day can accelerate wound healing [55]. As depicted in Fig. 3b, the WVTR of the bottle without film was 847.45 ± 41.45 g/m^2/day. The water vapor transmittance of PVA@PLA film is 551.62 ± 3.54 g/m^2/day, BSP-PVA@PLA film is 558.37 ± 12.70 g/m^2/day, RA-BSP@PLA film is 555.29 ± 7.02 g/ m^2/day. The diameter of water vapor is generally about 0.0004 μm [56], and the pore size of nanofibers is almost in the range of 0.01–10 μm diameter [57]. Accordingly, it can be argued that the blocking effect of the coaxial nanofibers on the water vapor is small, and meet the requirements of wound dressing WVTR, can be applied to wound healing.

3.6. Tensile strength

Good mechanical properties are essential for wound dressings, such that the stress-strain behavior of the coaxial nanofiber was tested, as presented in Fig. 4a and b. Notably, RA-BSP-PVA@PLA exhibited the right tensile strength and flexibility. The tensile strength of human skin ranged from 1 to 32 MPa, and its elongation at break fell into a range of 17 % to 27 % [58]. Displaying the mechanical characteristics of the prepared coaxial nanofibers (Fig. 4c and d). PVA@PLA displayed a tensile strength of 5.20 ± 0.14 MPa and an elongation at break of 40.13 ± 5.71 %, respectively. BSP-PVA@PLA exhibited a tensile strength of 9.08 ± 0.16 MPa and an elongation at a break of 44.43 ± 3.05 %. Tensile strength and elongation at break of RA-BSP-PVA@PLA coaxial nanofibers are 6.31 ± 0.10 MPa and 76.62 ± 4.51 %, respectively. Indicating that the prepared coaxial nanofibers have suitable

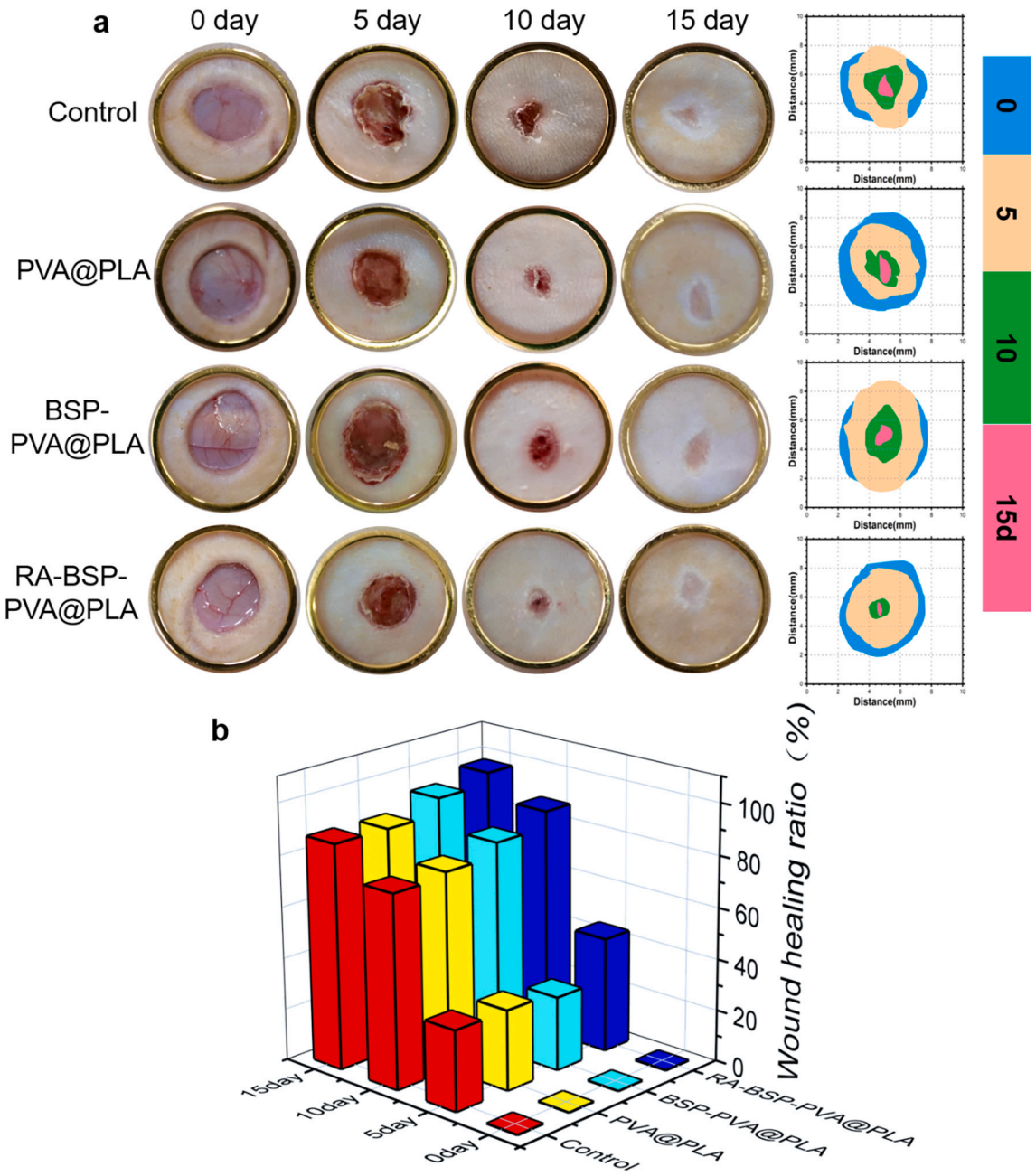

Fig. 6. Coaxial nanofibers promote wound healing. (a) Representative rat wound healing photos, as well as the wound healing between the control and treatment groups ($n = 3$). (b) Wound healing rate of control group and treatment group ($n = 3$).

mechanical properties and can be used in wound healing. Interestingly, compared with PVA@PLA, the mechanical properties of the nanofiber membrane were significantly enhanced after the addition of BSP, which may arise from the existence of numerous hydrogen bonds in the structure of BSP. Furthermore, the tensile strength of the fiber membrane was slightly reduced after the addition of RA in the core layer, whereas its elongation at break was increased.

The possible reason for the above-mentioned result is the increase in the number of hydrogen bonds between BSP and RA in the core layer solution. However, the two reacted with each other to reduce the formation of partial hydrogen bonds, thus resulting in the increase of elongation at break of coaxial nanofibers. This may be attributed to the increase in the number of hydrogen bonds between BSP and RA in the core layer solution, such that the mechanical properties of coaxial nanofibers were enhanced. However, the mechanical strength of nanofibers may also be related to the concentration of solution in the nuclear layer, which is the focus of further research.

3.7. Cell biocompatibility

Fibroblasts refer to the primary cells of the skin and take on a critical significance to the respective stage of wound healing. They are capable of increasing the speed of wound healing after injury. Moreover, the safety of coaxial nanofibers for fibroblasts was examined through cell apoptosis experiment, cell morphology experiment and MTT method [59] since the solution of PLA material is chloroform and DMF. Fig. 5a and b present the apoptosis of L929 cells after PVA@PLA, BSP-PVA@PLA and RA-BSP-PVA@PLA were co-cultured with L929 fibroblasts for 24 h, 48 h, and 72 h. Compared with the control group, only a small number of cells in the three types of fibroblasts were positive

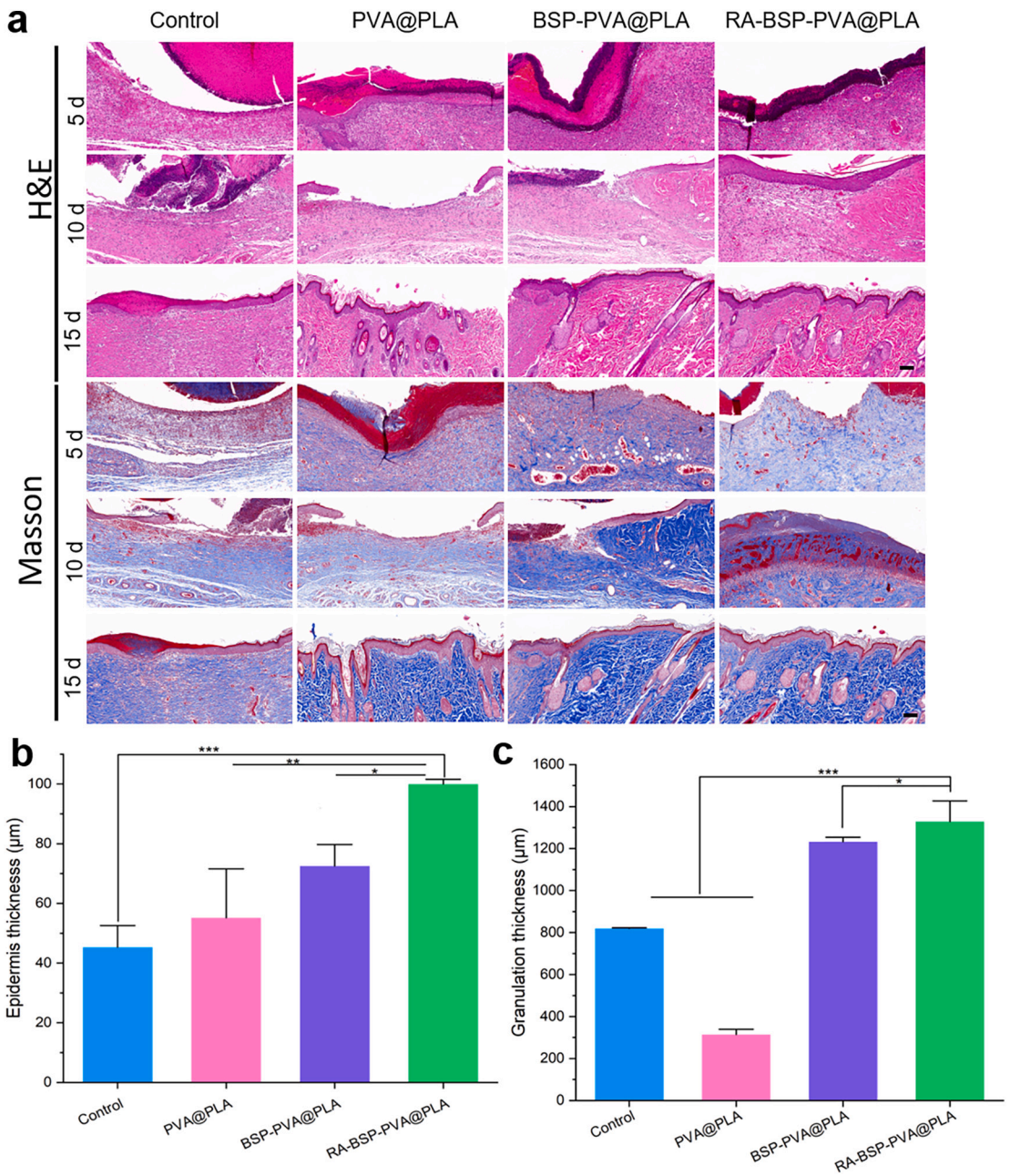

Fig. 7. Histologically stained images of wound tissue sections. (a) Representative images of wound tissue sections for H&E and Masson staining in the respective group. Scale bar: 100 μm. (b) Determining the epidermis' thickness (n = 3). (c) Different wounds' granulation tissue thickness (n = 3). Data are expressed as mean ± SD; $^{*}P < 0.05$, $^{**}P < 0.01$, and $^{***}P < 0.001$.

(bright blue). As depicted in Fig. 5c, L929 fibroblasts were spindle-shaped and did not change significantly after the co-culture of L929 fibroblasts with three coaxial nanofibers. As revealed by the above-mentioned results, the coaxial nanofibers do not affect the fibroblasts. The MTT experiment results still indicated a small toxic side effect, probably correlated with the precursor solution of spinning. However, compared with the control group, all exhibited good cell viability, higher than 90 % (Fig. 5d), suggesting that there was a slight difference in cell viability among the three groups. The above results suggested that, PVA@PLA, BSP-PVA@PLA, and RA-BSP-PVA@PLA exhibit good biocompatibility and safety properties.

3.8. Wound healing rate analysis

Wound healing rate has been proven as a vital metric for evaluating medical materials, and it can be adopted to determine the effectiveness of medical materials. Thus, a wound model was developed to assess wound healing. By analyzing the wound photos (Fig. 6a) after 5, 10, and 15 days of treatment, Image J software was used to measure the wound healing rate. The wound healed well in the RA-BSP-PVA@PLA group; both wound size and size healed after 5 and 10 days of treatment under the effect of RA-BSP-PVA@PLA on wound healing, whereas the healing was poor in the blank and PVA@PLA treatment groups. In the control group, the wound healing rate reached 31.06 ± 18.67 %, 75.13 ± 26.46 %, and 87.33 ± 9.68 % on the 5th, 10th, and 15th days (Fig. 6b), and large unhealed wounds were identified the healing rate exceeded 80 % on the 10th day after BSP-PVA@PLA and RA-BSP-PVA@PLA treatment. On the 15th day, RA and BSP reached 93.10 ± 5.45 % and 97.43 ± 2.98 %. The possible reason for this result is that RA and BSP in nanofibers can facilitate wound healing and anti-inflammatory. Accordingly, RA-

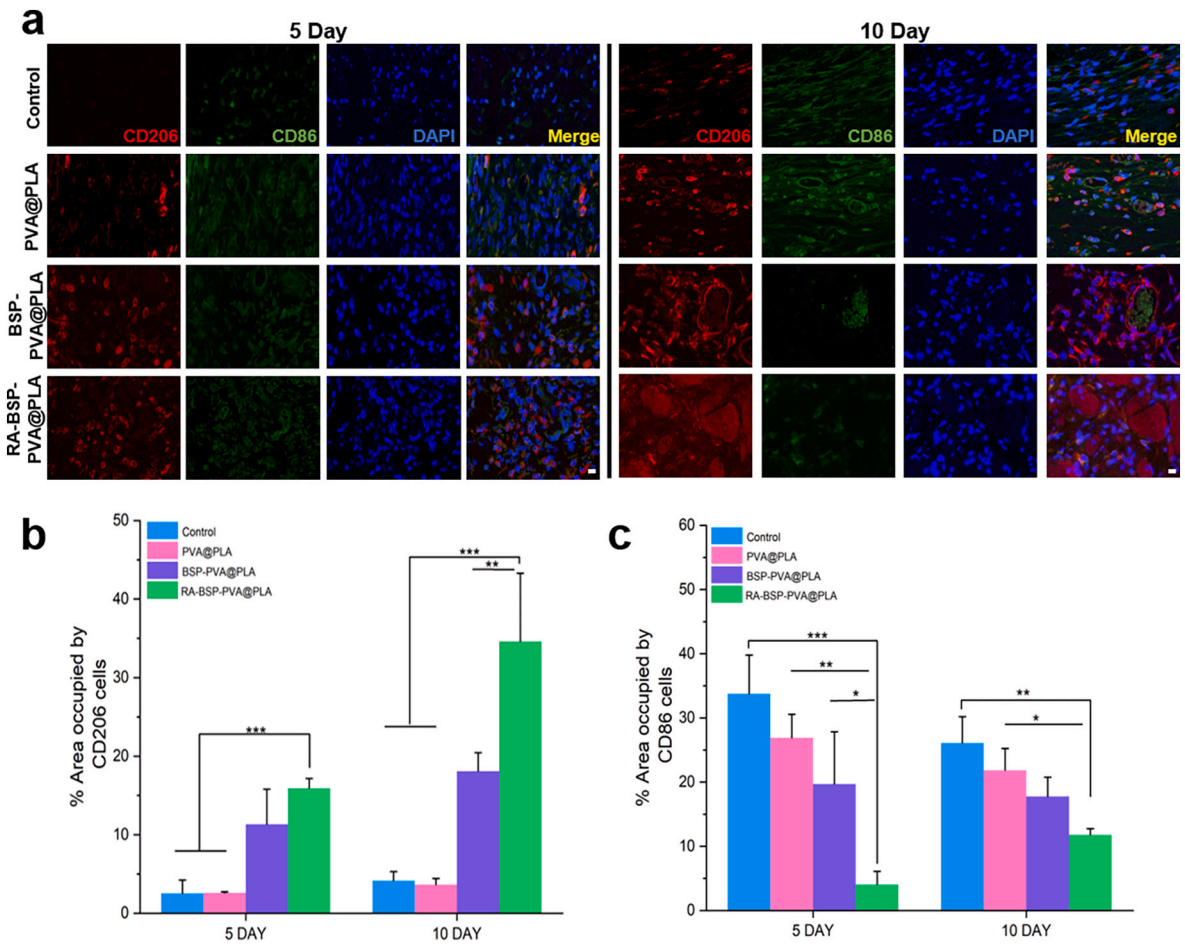

Fig. 8. Macrophages Polarization. (a) On the 5th and 10th days following therapy, immune-fluorescence was used to stain the wound tissue. Macrophages of the M1 and M2 phenotypes (CD86, green; CD206, red); and nuclei (DAPI, blue). Scale bar: 10 μm. (b) The percentage of M2 macrophages ($n = 3$). (c) The proportion of M1 macrophages (n = 3). Data represent mean ± SD; $^{*}P < 0.05$, $^{**}P < 0.01$, $^{***}P < 0.001$.

BSP-PVA@PLA is a potential medical material for a wound dressing that can expedite wound healing. However, the RA-BSP-PVA@PLA coaxial nanofibers only have the function of promoting wound healing, but lack antibacterial properties. Thus, the antibacterial properties of nanofibers by improving the nanofibers should be urgently enhanced. At the later stage, it is planned to add metal nano ions and other substances with good antibacterial properties, so as to achieve the versatile coaxial nanofibers exhibiting antibacterial and healing promoting effects.

3.9. Histopathological

The resultant profiles after H&E and Masson staining are depicted in Fig. 7a. On day 5, granulation tissue in the respective group indicated different levels of inflammation. In addition, the fibrin gum epithelium in the RA-BSP-PVA@PLA group was close to shutting down, and it was completely shut down on day 10. On the 15th day, a thick epidermal thickness was still identified in the blank group (Fig. 7b). For BSP-PVA@PLA and RA-BSP-PVA@PLA groups, the staining indicated dark blue and thick granulation tissue (Fig. 7c). The above results suggested that RA-BSP-PVA@PLA can effectively treat wounds while expediting wound healing.

3.10. Macrophage polarization and inflammatory reaction in wound

3.10.1. Macrophages are polarized

Inflammation has been confirmed as an essential phase of wound healing is inflammation. CD86 and CD206 were served as markers of M1 and M2 macrophages to evaluate the degree of alterations in wound inflammation brought on by various coaxial nanofibers [60]. Fig. 8a depicts the immunofluorescence labeling of wound macrophages expressing CD86 and CD206 at days 5 and 10 after therapy. As indicated by the results (Fig. 8b and c) showed that the expression of M2 macrophages (CD206) in the wound on the 5th day after RA-BSP-PVA@PLA treatment reached the maximum among the four groups, and the expression of CD206 in BSP-PVA@PLA was higher than that in the control group and PVA@PLA, whereas the CD86 level in the control group was the highest and the CD206 level was lower. This may be related to the function that both BSP and RA have in inducing macrophage polarization. On day 10 after treatment, the expression of CD86 in wound macrophages was down-regulated, whereas CD206 expression was up-regulated slightly. The control group remained in the inflammatory phase on day 10 and could not go on to the subsequent stage of healing since they achieved the highest level of CD86 and the lowest level of CD206 of these.

3.10.2. Inflammatory reaction in wound

MPO^{+} refers to one of the indicators capable determining the level of inflammation in a wound [61]. Accordingly, the expression of MPO^{+} in wound tissue after treatment with three coaxial nanofibers was employed as an evaluation criterion for the anti-inflammatory properties of coaxial nanofibers. Fig. 9a presents the expression of MPO^{+} in the wound tissue at day 5 and day 10 after treatment. As depicted in Fig. 9b and c, the granulation tissue of the wound was surrounded by MPO^{+}neutrophils on days 5 and 10 in the blank control group,

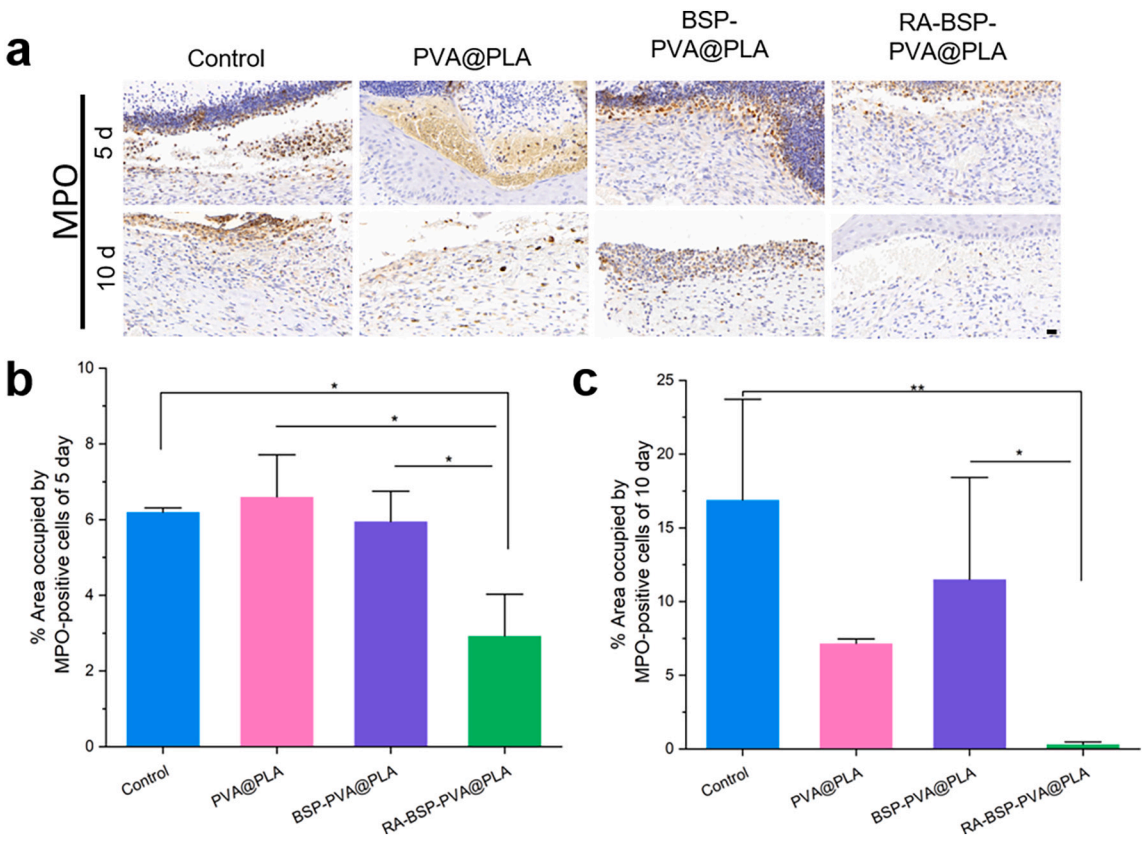

Fig. 9. Expression of MPO^+ in wound inflammation. (a) Representative MPO^+ (neutrophil) images of wound tissue after 5 and 10 days of treatment. Scale bar: 50 μm. (b) MPO^+ neutrophils after day 5 ($n = 3$). (c) MPO^+ neutrophils after day 10 (n = 3). Data represent mean ± SD; $^*P < 0.05$, $^{**}P < 0.01$.

suggesting that there were still more permanent inflammatory factors in the above-mentioned wounds. However, in RA-BSP-PVA@PLA, fewer neutrophils were remaining on day 5 compared with the other three groups. Besides, on the 10th day, a higher density of neutrophils was identified in the blank control group, PVA@PLA, and BSP-PVA@PLA groups, which proved that the inflammation was still sustained, but only a small number of neutrophils remained in the RA-BSP-PVA@PLA group, thus further confirming the function of RA in improving wound inflammation.

4. Conclusion

In brief, in terms of RA-BSP-PVA@PLA, the results indicated that the average diameter of the fiber was uniform without beaded particles. The addition of BSP and RA significantly enhanced the mechanical properties of the coaxial fiber, probably correlated with the number of hydrogen bonds between molecules. Compared with the control group, RA-BSP-PVA@PLA showed excellent biocompatibility. Using the rat model, it has demonstrated that it has the potential to enhance wound healing. In addition, the histological examination showed that the collagen deposition was favorable, epidermal thickness and granulation tissue recovered adequately, and that the addition of RA could cooperate with BSP to promote the conversion of M1 macrophages into M2 macrophages, reduce the release of inflammatory factors, and promote effective wound healing.

As a result, the coaxial fibers developed in this study have the potential to be employed as wound dressings in clinical settings. They are safe, efficient, stable, and capable of promoting wound healing.

CRediT authorship contribution statement

Guofeng Zhong: Conceptualization, Investigation, Experiment, Writing Original Draft.

Mengyu Qiu: Conceptualization, Experiment.

Junbo Zhang: Investigation, Revising the manuscript.

Fuchen Jiang: Validation, Resources.

Xuan Yue: Instruction the experiment Date.

Chi Huang: Curation, Experiment, Software.

Shiyi Zhao: Investigation, Instruction the experiment Date.

Chen Zhang: Supervision, Formal analysis, Writing-review & Editing.

Yan Qu: Supervision, Formal analysis.

Declaration of competing interest

The authors declare that they have no known competing financial interests or personal relationships that could have appeared to influence the work reported in this paper.

Acknowledgments

This study was supported by China Postdoctoral Science Foundation (2021M690488), Health Commission of Sichuan Province (21PJ108), Innovation Team and Talents Cultivation Program of National Administration of Traditional Chinese Medicine (ZYYCXTD-D-202209), Natural Science Youth Foundation of Sichuan Province (23NSFSC1768), The Central Guidance on Local Science and Technology Development Fund of Sichucan (No. 2022ZYD0099, China).

Appendix A. Supplementary data

Supplementary data to this article can be found online at https://doi.org/10.1016/j.ijbiomac.2023.123693.

References

[1] P. Kolimi, S. Narala, D. Nyavanandi, A.A.A. Youssef, N. Dudhipala, Innovative treatment strategies to accelerate wound healing: trajectory and recent advancements, Cells 11 (15) (2022).

[2] B.S. Kim, Y.W. Kwon, J.S. Kong, G.T. Park, G. Gao, W. Han, M.B. Kim, H. Lee, J. H. Kim, D.W. Cho, 3D cell printing of in vitro stabilized skin model and in vivo pre-vascularized skin patch using tissue-specific extracellular matrix bioink: a step towards advanced skin tissue engineering, Biomaterials 168 (2018) 38–53.

[3] R.S. Sequeira, S.P. Miguel, C.S.D. Cabral, A.F. Moreira, P. Ferreira, I.J. Correia, Development of a poly(vinyl alcohol)/lysine electrospun membrane-based drug delivery system for improved skin regeneration, Int. J. Pharm. 570 (2019), 118640.

[4] R.S. Bhattarai, R.D. Bachu, S.H.S. Boddu, S. Bhaduri, Biomedical applications of electrospun nanofibers: drug and nanoparticle delivery, Pharmaceutics 11 (1) (2018).

[5] B.N. Blackstone, J.M. Hahn, K.L. McFarland, D.M. DeBruler, D.M. Supp, H. M. Powell, Inflammatory response and biomechanical properties of coaxial scaffolds for engineered skin in vitro and post-grafting, Acta Biomater. 80 (2018) 247–257.

[6] L. Cao, Q. Liu, J. Ren, W. Chen, Y. Pei, D.L. Kaplan, S. Ling, Electro-blown spun Silk/Graphene nanoionotronic skin for multifunctional fire protection and alarm, Adv. Mater. 33 (38) (2021), e2102500.

[7] C. Gao, L. Zhang, J. Wang, M. Jin, Q. Tang, Z. Chen, Y. Cheng, R. Yang, G. Zhao, Electrospun nanofibers promote wound healing: theories, techniques, and perspectives, J. Mater. Chem. B 9 (14) (2021) 3106–3130.

[8] Y. Han, J. Ding, J. Zhang, Q. Li, H. Yang, T. Sun, H. Li, Fabrication and characterization of polylactic acid coaxial antibacterial nanofibers embedded with cinnamaldehyde/tea polyphenol with food packaging potential, Int. J. Biol. Macromol. 184 (2021) 739–749.

[9] S. Jin, R. Yang, C. Chu, C. Hu, Q. Zou, Y. Li, Y. Zuo, Y. Man, J. Li, Topological structure of electrospun membrane regulates immune response, angiogenesis and bone regeneration, Acta Biomater. 129 (2021) 148–158.

[10] K. Chen, H. Pan, D. Ji, Y. Li, H. Duan, W. Pan, Curcumin-loaded sandwich-like nanofibrous membrane prepared by electrospinning technology as wound dressing for accelerate wound healing, Mater. Sci. Eng. C Mater. Biol. Appl. 127 (2021), 112245.

[11] M. Yu, Y. Du, Y. Han, B. Lei, Biomimetic elastomeric bioactive siloxane-based hybrid nanofibrous scaffolds with miRNA activation: a joint physico-chemical-biological strategy for promoting bone regeneration, Adv. Funct. Mater. 30 (4) (2019).

[12] P. Rathore, J.D. Schiffman, Beyond the single-nozzle: coaxial electrospinning enables innovative nanofiber chemistries, geometries, and applications, ACS Appl. Mater. Interfaces 13 (1) (2021) 48–66.

[13] J. Yoon, H.S. Yang, B.S. Lee, W.R. Yu, Recent Progress in coaxial electrospinning: new parameters, various structures, and wide applications, Adv. Mater. 30 (42) (2018), e1704765.

[14] M. Wang, Y. Wang, E. Omari-Siaw, S. Wang, Y. Zhu, X. Xu, Reduced burst release and enhanced Oral bioavailability in shikimic acid-loaded polylactic acid submicron particles by coaxial electrospray, J. Pharm. Sci. 105 (8) (2016) 2427–2436.

[15] M.R. Zare, M. Khorram, S. Barzegar, F. Asadian, Z. Zareshahrabadi, M.J. Saharkhiz, S. Ahadian, K. Zomorodian, Antimicrobial core-shell electrospun nanofibers containing ajwain essential oil for accelerating infected wound healing, Int. J. Pharm. 603 (2021), 120698.

[16] K.T. Shalumon, C. Sheu, C.H. Chen, S.H. Chen, G. Jose, C.Y. Kuo, J.P. Chen, Multi-functional electrospun antibacterial core-shell nanofibrous membranes for prolonged prevention of post-surgical tendon adhesion and inflammation, Acta Biomater. 72 (2018) 121–136.

[17] Y. He, Z. Chen, X. Nie, D. Wang, Q. Zhang, T. Peng, C. Zhang, D. Wu, J. Zhang, Recent advances in polysaccharides from edible and medicinal polygonati rhizoma: from bench to market, Int. J. Biol. Macromol. 195 (2022) 102–116.

[18] C. Zhang, X. Wang, M. Xiao, J. Ma, Y. Qu, L. Zou, J. Zhang, Nano-in-micro alginate/chitosan hydrogel via electrospray technology for orally curcumin delivery to effectively alleviate ulcerative colitis, Mater. Des. 221 (2022).

[19] J. Wang, L. Tian, L. He, N. Chen, S. Ramakrishna, K.F. So, X. Mo, Lycium barbarum polysaccharide encapsulated poly lactic-co-glycolic acid nanofibers: cost effective herbal medicine for potential application in peripheral nerve tissue engineering, Sci. Rep. 8 (1) (2018) 8669.

[20] T. Ponrasu, B.H. Chen, T.H. Chou, J.J. Wu, Y.S. Cheng, Fast dissolving electrospun nanofibers fabricated from jelly fig Polysaccharide/Pullulan for drug delivery applications, Polymers (Basel) 13 (2) (2021).

[21] R. Yang, D. Wang, H. Li, Y. He, X. Zheng, M. Yuan, M. Yuan, Preparation and characterization of Bletilla striata polysaccharide/polylactic acid composite, Molecules 24 (11) (2019).

[22] Z. Li, R. Zeng, L. Yang, X. Ren, K.G. Maffucci, Y. Qu, Development and characterization of PCL electrospun membrane-coated Bletilla striata polysaccharide-based gastroretentive drug delivery system, AAPS PharmSciTech 21 (2) (2020) 66.

[23] Q. Zhang, C. Qi, H. Wang, X. Xiao, Y. Zhuang, S. Gu, Y. Zhou, L. Wang, H. Yang, W. Xu, Biocompatible and degradable Bletilla striata polysaccharide hemostasis sponges constructed from natural medicinal herb Bletilla striata, Carbohydr. Polym. 226 (2019), 115304.

[24] P. Zhou, S. Zhao, C. Huang, Y. Qu, C. Zhang, Bletilla striata polysaccharide microneedle for effective transdermal administration of model protein antigen, Int. J. Biol. Macromol. 205 (2022) 511–519.

[25] C. Chen, P. Zhou, C. Huang, R. Zeng, L. Yang, Z. Han, Y. Qu, C. Zhang, Photothermal-promoted multi-functional dual network polysaccharide hydrogel adhesive for infected and susceptible wound healing, Carbohydr. Polym. 273 (2021), 118557.

[26] S.H. Chen, P.Y. Chou, Z.Y. Chen, D.C. Chuang, S.T. Hsieh, F.H. Lin, An electrospun nerve wrap comprising Bletilla striata polysaccharide with dual function for nerve regeneration and scar prevention, Carbohydr. Polym. 250 (2020), 116981.

[27] Y. Li, Z. Ma, X. Yang, Y. Gao, Y. Ren, Q. Li, Y. Qu, G. Chen, R. Zeng, Investigation into the physical properties, antioxidant and antibacterial activity of Bletilla striata polysaccharide/chitosan membranes, Int. J. Biol. Macromol. 182 (2021) 311–320.

[28] G. Rivera-Hernandez, M. Antunes-Ricardo, P. Martinez-Morales, M.L. Sanchez, Polyvinyl alcohol based-drug delivery systems for cancer treatment, Int. J. Pharm. 600 (2021), 120478.

[29] J. Ahlawat, V. Kumar, P. Gopinath, Carica papaya loaded poly (vinyl alcohol)-gelatin nanofibrous scaffold for potential application in wound dressing, Mater. Sci. Eng. C Mater. Biol. Appl. 103 (2019), 109834.

[30] M.Z.-H.Yang Kai, Li Yuan, Gao Yuan-ping, Yang Xiao, Zeng Rui, Zhang Ji-zhong, He Xin, W. Yi-han, Box-Behnken response surface method optimized BSP/PVA wet spinning process and fiber performance evaluation, Chin. Traditional and Herbal Drugs 51 (14) (2020) 3645–3654.

[31] M. Santoro, S.R. Shah, J.L. Walker, A.G. Mikos, Poly(lactic acid) nanofibrous scaffolds for tissue engineering, Adv. Drug Deliv. Rev. 107 (2016) 206–212.

[32] J. Lin, S. Luo, C. Yang, Y. Xiao, L. Yang, Z. Wang, Bio-based polymeric hemostatic material and wound dressing, Prog. Chem. 33 (4) (2022) 583–595.

[33] R. Ramalingam, C. Dhand, V. Mayandi, C.M. Leung, H. Ezhilarasu, S. K. Karuppannan, P. Prasannan, S.T. Ong, N. Sunderasan, I. Kaliappan, M. Kamruddin, V.A. Barathi, N.K. Verma, S. Ramakrishna, R. Lakshminarayanan, K.D. Arunachalam, Core-Shell structured antimicrobial nanofiber dressings containing herbal extract and antibiotics combination for the prevention of biofilms and promotion of cutaneous wound healing, ACS Appl. Mater. Interfaces 13 (21) (2021) 24356–24369.

[34] X. Lan, Y. Liu, Y. Wang, F. Tian, X. Miao, H. Wang, Y. Tang, Coaxial electrospun PVA/PCL nanofibers with dual release of tea polyphenols and epsilon-poly (L-lysine) as antioxidant and antibacterial wound dressing materials, Int. J. Pharm. 601 (2021), 120525.

[35] M. Murariu, P. Dubois, PLA composites: from production to properties, Adv. Drug Deliv. Rev. 107 (2016) 17–46.

[36] M. Hajikhani, Z. Emam-Djomeh, G. Askari, Fabrication and characterization of mucoadhesive bioplastic patch via coaxial polylactic acid (PLA) based electrospun nanofibers with antimicrobial and wound healing application, Int. J. Biol. Macromol. 172 (2021) 143–153.

[37] P. Chhabra, G. Chauhan, A. Kumar, Augmented healing of full thickness chronic excision wound by rosmarinic acid loaded chitosan encapsulated graphene nanopockets, Drug Dev. Ind. Pharm. 46 (6) (2020) 878–888.

[38] F.N.S. Fachel, M. Dal Pra, J.H. Azambuja, M. Endres, V.L. Bassani, L.S. Koester, A. T. Henriques, A.G. Barschak, H.F. Teixeira, E. Braganhol, Glioprotective effect of chitosan-coated rosmarinic acid nanoemulsions against lipopolysaccharide-induced inflammation and oxidative stress in rat astrocyte primary cultures, Cell. Mol. Neurobiol. 40 (1) (2020) 123–139.

[39] M.C. Kuba, A. Turkoglu, A. Oguz, M.C. Tuncer, S. Kaya, O. Basol, H. Bilge, F. Tatli, Comparison of local rosmarinic acid and topical dexpanthenol applications on wound healing in a rat experimental wound model, Folia Morphol. (Warsz) 80 (3) (2021) 618–624.

[40] Z. Song, H. Xiao, Y. Zhao, Hydrophobic-modified nano-cellulose fiber/PLA biodegradable composites for lowering water vapor transmission rate (WVTR) of paper, Carbohydr. Polym. 111 (2014) 442–448.

[41] W.F. de Deus, B.M. de Franca, J.S.B. Forero, A.E.C. Granato, H. Ulrich, A. Doria, M. M. Amaral, A. Slabon, B.V.M. Rodrigues, Curcuminoid-tailored interfacial free energy of hydrophobic fibers for enhanced biological properties, ACS Appl. Mater. Interfaces 13 (21) (2021) 24493–24504.

[42] Z. Li, K.M. Bratlie, The influence of polysaccharides-based material on macrophage phenotypes, Macromol. Biosci. 21 (8) (2021), e2100031.

[43] P. Mai, C. Chen, X. Xiao, X. Ma, Y. Shi, G. Miao, L. Zhang, Rosmarinic acid protects against ulcerative colitis by regulating macrophage polarization depending on heme oxygenase-1 in mice, Eur. J. Inflamm. 18 (2020).

[44] J. Liu, M. Qu, C. Wang, Y. Xue, H. Huang, Q. Chen, W. Sun, X. Zhou, G. Xu, X. Jiang, A dual-cross-linked hydrogel patch for promoting diabetic wound healing, Small 18 (17) (2022), e2106172.

[45] M. Huerta-Madronal, J. Caro-Leon, E. Espinosa-Cano, M.R. Aguilar, B. Vazquez-Lasa, Chitosan - rosmarinic acid conjugates with antioxidant, anti-inflammatory and photoprotective properties, Carbohydr. Polym. 273 (2021), 118619.

[46] Z. Chen, L. Cheng, Y. He, X. Wei, Extraction, characterization, utilization as wound dressing and drug delivery of Bletilla striata polysaccharide: a review, Int. J. Biol. Macromol. 120 (Pt B) (2018) 2076–2085.

[47] T.Q. Bao, Y. Li, C. Qu, Z.G. Zheng, H. Yang, P. Li, Antidiabetic effects and mechanisms of rosemary (Rosmarinus officinalis L.) and its phenolic components, Am. J. Chin. Med. 48 (6) (2020) 1353–1368.

[48] Z. Liao, R. Zeng, L. Hu, K.G. Maffucci, Y. Qu, Polysaccharides from tubers of Bletilla striata: physicochemical characterization, formulation of buccoadhesive wafers and preliminary study on treating oral ulcer, Int. J. Biol. Macromol. 122 (2019) 1035–1045.

[49] M. Naseri-Nosar, S. Farzamfar, H. Sahrapeyma, S. Ghorbani, F. Bastami, A. Vaez, M. Salehi, Cerium oxide nanoparticle-containing poly (epsilon-caprolactone)/gelatin electrospun film as a potential wound dressing material: in vitro and in vivo evaluation, Mater. Sci. Eng. C Mater. Biol. Appl. 81 (2017) 366–372.

[50] P. Patil, KAR, JTM, ACP, MAC, B.R. Dollinger, CRD, MKG, RDA, JMC, F. Yu, MGB, JRM, NLC, JMD, C.M. Thompson, AB, AHH, SAG, CLD, Reactive oxygen species–degradable polythioketal urethane foam dressings to promote porcine skin wound repair, Sci. Transl. Medicine 14 (641) (2022) 1–18.
[51] X. Li, F. Xu, Y. He, Y. Li, J. Hou, G. Yang, S. Zhou, A hierarchical structured ultrafine fiber device for preventing postoperative recurrence and metastasis of breast cancer, Adv. Funct. Mater. 30 (45) (2020).
[52] T.N. da Silva, R.P. Goncalves, C.L. Rocha, B.S. Archanjo, C.A.G. Barboza, M.B. R. Pierre, F. Reynaud, P.H. de Souza Picciani, Controlling burst effect with PLA/PVA coaxial electrospun scaffolds loaded with BMP-2 for bone guided regeneration, Mater. Sci. Eng. C Mater. Biol. Appl. 97 (2019) 602–612.
[53] Y. Qin, H. Shen, L. Han, Z. Zhu, F. Pan, S. Yang, X. Yin, Mechanically robust janus Poly(lactic acid) hybrid fibrous membranes toward highly efficient switchable separation of surfactant-stabilized oil/water emulsions, ACS Appl. Mater. Interfaces 12 (45) (2020) 50879–50888.
[54] M.V. Vellayappan, J.R. Venugopal, S. Ramakrishna, S. Ray, A.F. Ismail, M. Mandal, A. Manikandan, S. Seal, S.K. Jaganathan, Electrospinning applications from diagnosis to treatment of diabetes, RSC Adv. 6 (87) (2016) 83638–83655.
[55] X. Chen, X. Wang, S. Wang, X. Zhang, J. Yu, C. Wang, Mussel-inspired polydopamine-assisted bromelain immobilization onto electrospun fibrous membrane for potential application as wound dressing, Mater. Sci. Eng. C Mater. Biol. Appl. 110 (2020), 110624.
[56] Y. Yue, X. Gong, W. Jiao, Y. Li, X. Yin, Y. Si, J. Yu, B. Ding, In-situ electrospinning of thymol-loaded polyurethane fibrous membranes for waterproof, breathable, and antibacterial wound dressing application, J. Colloid Interface Sci. 592 (2021) 310–318.
[57] J. Rnjak-Kovacina, A.S. Weiss, Increasing the pore size of electrospun scaffolds, Tissue Eng. Part B Rev. 17 (5) (2011) 365–372.
[58] J.R. Dias, P.L. Granja, P.J. Bártolo, Advances in electrospun skin substitutes, Prog. Mater. Sci. 84 (2016) 314–334.
[59] R. Revati, M.S.A. Majid, M.J.M. Ridzuan, N. Mamat, E.M. Cheng, H.A. Alshahrani, In vitro biodegradation, cytotoxicity, and biocompatibility of polylactic acid/napier cellulose nanofiber scaffold composites, Int. J. Biol. Macromol. 223 (Pt A) (2022) 479–489.
[60] W. Zhao, X. Zhang, R. Zhang, K. Zhang, Y. Li, F.J. Xu, Self-assembled herbal medicine encapsulated by an oxidation-sensitive supramolecular hydrogel for chronic wound treatment, ACS Appl. Mater. Interfaces 12 (51) (2020) 56898–56907.
[61] W. Zhu, J. Mei, X. Zhang, J. Zhou, D. Xu, Z. Su, S. Fang, J. Wang, X. Zhang, C. Zhu, Photothermal nanozyme-based microneedle patch against refractory bacterial biofilm infection via iron-actuated Janus ion therapy, Adv. Mater. 34 (51) (2022), e2207961.